J. Fluid Mech. (2019), *vol.* 863, *pp.* 242–268.
doi:10.1017/jfm.2018.945

An analytical model for asymmetric Mach reflection configuration in steady flows

Shobhan Roy[1] **and Rajesh Gopalapillai**[1,†]

[1]Department of Aerospace Engineering, Indian Institute of Technology Madras, Chennai, Tamil Nadu 600036, India

(Received 19 April 2018; revised 3 November 2018; accepted 21 November 2018; first published online 23 January 2019)

An analytical model is presented for the configuration of Mach reflection (MR) due to the interaction of two-dimensional steady supersonic flow over asymmetric wedges. The present asymmetric MR model is an extension of an earlier model for the symmetric MR configuration. The overall Mach reflection (oMR) in the asymmetric wedge configuration is analysed as a combination of upper and lower half-domains of symmetric reflection configurations. Suitable assumptions are made to close the combined set of equations. The subsonic pocket downstream of the Mach stem is taken to be oriented along an average inclination, based on the streamline deflections by the Mach stem at the triple points. This assumption is found to give satisfactory results for all types of oMR configurations. The oMR configuration is predicted for all types of reflections such as direct Mach reflection (DiMR), stationary Mach reflection (StMR) and inverse Mach reflection (InMR). The reflection configuration and Mach stem shape given by the model for various sets of wedge angles, especially those giving rise to InMR, have been predicted and validated with the available numerical and experimental data. The von Neumann criterion for oMR is accurately predicted by this model. The asymmetric Mach stem profile is well captured. The variation of Mach stem height with wedge angle is also analysed and it is found that simplification of an asymmetric MR to a symmetric MR leads to over-prediction of the Mach stem height and hence the extent of the subsonic region.

Key words: compressible flows, gas dynamics, shock waves

1. Introduction

Shock reflection phenomena can be seen in many practical engineering applications involving supersonic flows. Shock reflections are broadly classified as regular reflections (RR) and irregular reflections (IR). In steady flows, IR occurs most commonly as Mach reflection (MR). Figure 1(*a*,*b*) shows the schematics of RR and MR respectively. It is known from classical shock reflection theory (Ben-Dor 2007) that an RR occurs when the reflected shock wave (*r*) is capable of producing an equal flow deflection in the opposite direction to that produced by the incident shock wave (*i*). On the other hand, if the reflected shock wave is not able to produce an equal deflection to that produced by the incident shock wave, an MR is formed. It is

†Email address for correspondence: rajesh@ae.iitm.ac.in

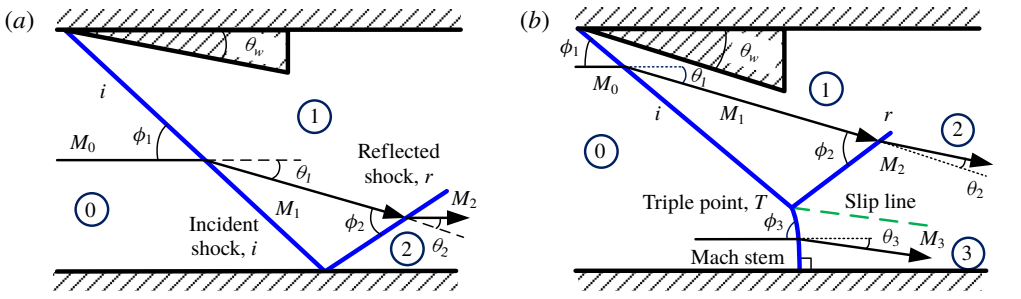

FIGURE 1. (Colour online) (*a*) Regular reflection for $\theta_w < \theta_w^D(M_1) < \theta_w^D(M_0)$; (*b*) Mach reflection for $\theta_w^D(M_1) < \theta_w < \theta_w^D(M_0)$; where subscript w denotes wedge and superscript D denotes detachment criterion.

seen that the shock configurations of RR and MR are very different from each other and consequently, the transition RR↔MR brings forth significant changes in the flow field.

It was widely accepted that there are two limiting criteria for RR↔MR transition in steady flows, namely the von Neumann and the detachment criteria (Von-Neumann 1943, 1945; Henderson & Lozzi 1975; Hornung, Oertel & Sandeman 1979). The von Neumann criterion suggests that the RR↔MR transition occurs when the static pressures downstream of the reflected shock and the Mach stem match at the triple point. The detachment criterion proposes that RR↔MR transition happens when the required turning angle for the flow downstream of the incident shock to become parallel to the reflecting surface, exceeds the maximum turning angle possible for that flow Mach number. Above the wedge angle corresponding to the detachment criterion, only MR structure exists, and below the wedge angle corresponding to von Neumann criterion, only RR structure exists.

It has been found from all the previous studies that the wedge-angle-variation-induced transition of RR→MR is abrupt, in the sense that the Mach stem (followed by a region of subsonic flow) appears suddenly. On the other hand, the MR→RR transition is smooth, with the Mach stem height gradually reducing to zero. In other words, the reduction of the Mach stem size to zero presents itself as a corollary to the MR→RR transition criterion, where the von Neumann condition is satisfied. This led the researchers to the prediction of the height of the Mach stem and the overall MR configuration through geometric considerations, to identify the von Neumann criterion for transition. Efforts towards determining the Mach reflection configurations started with Azevedo (1989). He analytically modelled a symmetric MR, as shown in figure 2. In this work, it was assumed that the leading characteristic from the expansion fan (emanating from the trailing edge of the wedge and transmitted by the reflected shock) interacts with the slip line at the sonic throat. This point is shown as F in figure 2. The slip line is taken to be straight until this point.

Li & Ben-Dor (1997) improved this symmetric model by considering additional flow features such as the interaction of the reflected shock with the expansion fan from the trailing edge of the wedge, the entropy layer emanating from this interaction and the reflection of the expansion fan from the slip line. In this model, the slip line starts curving from point F onward and becomes parallel to the symmetry plane at a point where the central characteristic of the expansion fan interacts with the slip line and also the sonic throat occurs. They employed a second-order curve to model the curved entities like the Mach stem and segments of the slip line and the reflected shock.

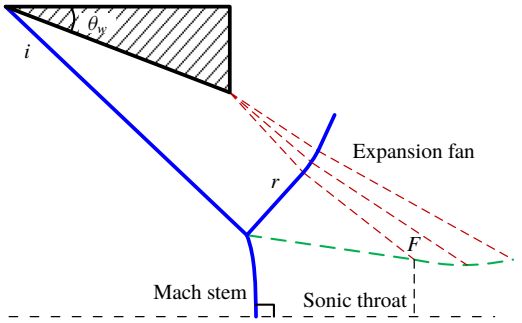

FIGURE 2. (Colour online) Model for Mach reflection configuration (Azevedo 1989).

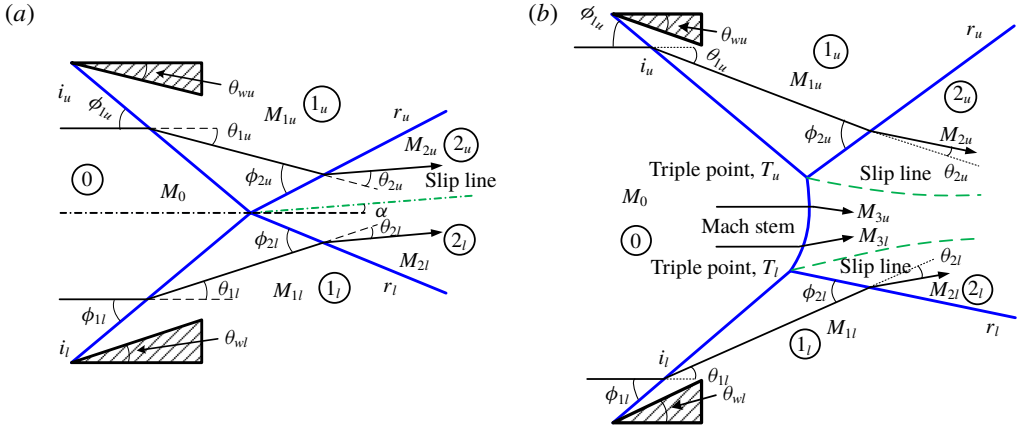

FIGURE 3. (Colour online) Types of asymmetric reflection: (*a*) oRR (overall regular reflection); (*b*) oMR (overall Mach reflection); subscript *u* stands for upper domain and *l* stands for lower domain.

Mouton (2007), Hornung & Mouton (2008) and Mouton & Hornung (2008) suggested another model for symmetric MR, where they considered only the geometrical features of the flow problem and omitted the curvature of the discontinuities (Mach stem, slip line). Further minute details of the MR configuration were considered in more recent models by Gao & Wu (2010) and Bai & Wu (2017) to predict the MR configuration. Both these models incorporated the presence of secondary waves emanating from the slip line into the non-uniform supersonic flow and consequent interactions therewith, leading to an inflection in the slip-line curve at point F. Bai & Wu (2017) additionally found a discontinuity in the slope of the slip line.

For most practical cases of engineering interest such as supersonic inlet flows, nozzle flows and hypersonic flows, the type of MR is asymmetric rather than symmetric. Two types of configuration are generally observed in asymmetric reflections – overall regular reflection (oRR) and overall Mach reflection (oMR) (Li, Chpoun & Ben-Dor 1999; Ben-Dor 2007). The schematics are given in figure 3. The subscripts u and l indicate upper and lower regions, respectively.

Mouton (2007) defined an equivalence angle to estimate the Mach stem height for asymmetric MR from their symmetric MR model. Recently, Roy & Rajesh (2017) presented an analytical model for asymmetric MR based on the Li & Ben-Dor (1997)

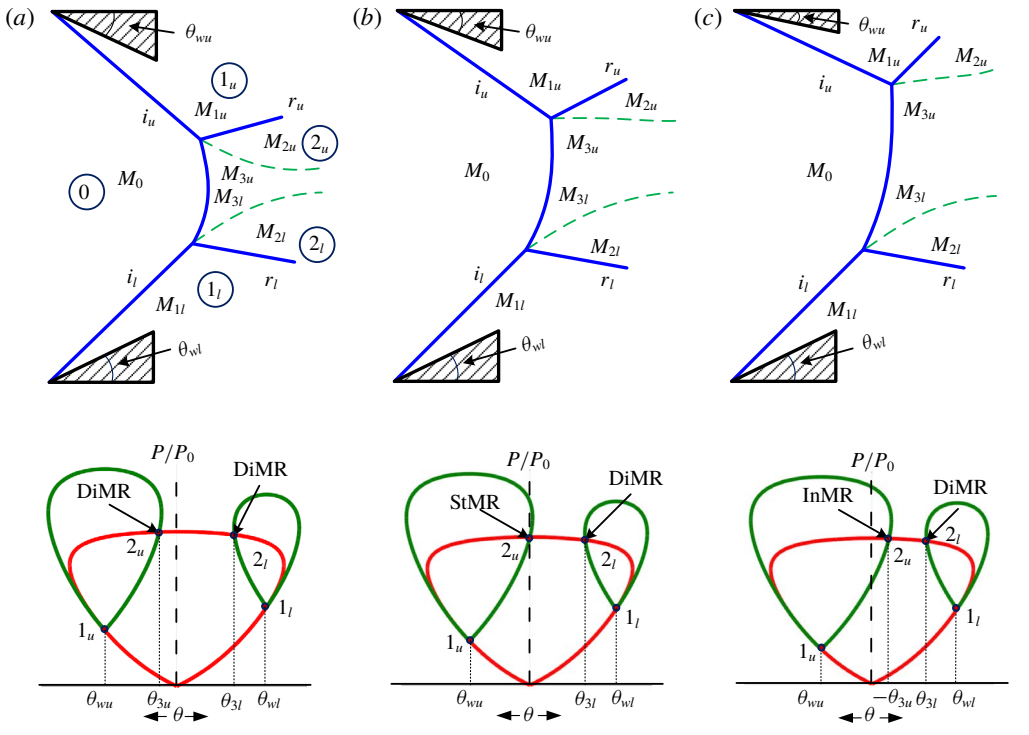

FIGURE 4. (Colour online) Types of overall Mach reflection (based on upper wedge angle): (*a*) DiMR (direct Mach reflection); (*b*) StMR (stationary Mach reflection); (*c*) InMR (inverse Mach reflection).

model. Tao *et al.* (2017) proposed a model for asymmetric MR, based on the Gao & Wu (2010) symmetric MR model. They claimed that the locations of the triple points are a function of the angles of the two slip lines, which they based on the experimental visualisations of oMR (Tao, Fan & Zhao 2015) for some particular conditions. The model takes into consideration the secondary waves on the slip lines as in the case of Gao & Wu (2010) and the predictions are shown to be in reasonable agreement with previous experimental and numerical data. However, the estimation of Mach stem height for various oMR configurations (figure 4) in the asymmetric wedge-angle–Mach-number domain was never attempted in their work.

Figure 4 shows various configurations of oMR in the wedge-angle–Mach-number domain, along with the corresponding shock polars based on the inclinations of the slip line (Li *et al.* 1999; Ben-Dor 2007). As can be seen from the figure, the InMR configuration is very different from the other oMR configurations. For example, it is not possible to have two InMRs in an oMR as that would result in diverging slip lines and hence render the flow non-physical. InMR is a discrete manifestation only in asymmetric reflection in steady flows.

Various configurations of asymmetric reflection can be better understood with the help of the (θ_{wu}, θ_{wl})-plane, as given in figure 5(*a*) for an incoming Mach number M_0 of 4.96 (Li *et al.* 1999). The figure shows the plots of detachment (θ_w^D) and von Neumann (θ_w^N) criteria, and the domains of various shock reflections that are theoretically possible for a given set of wedge angles. The region enclosed between the curves demarcates the dual-solution domain, whereby both oRR and

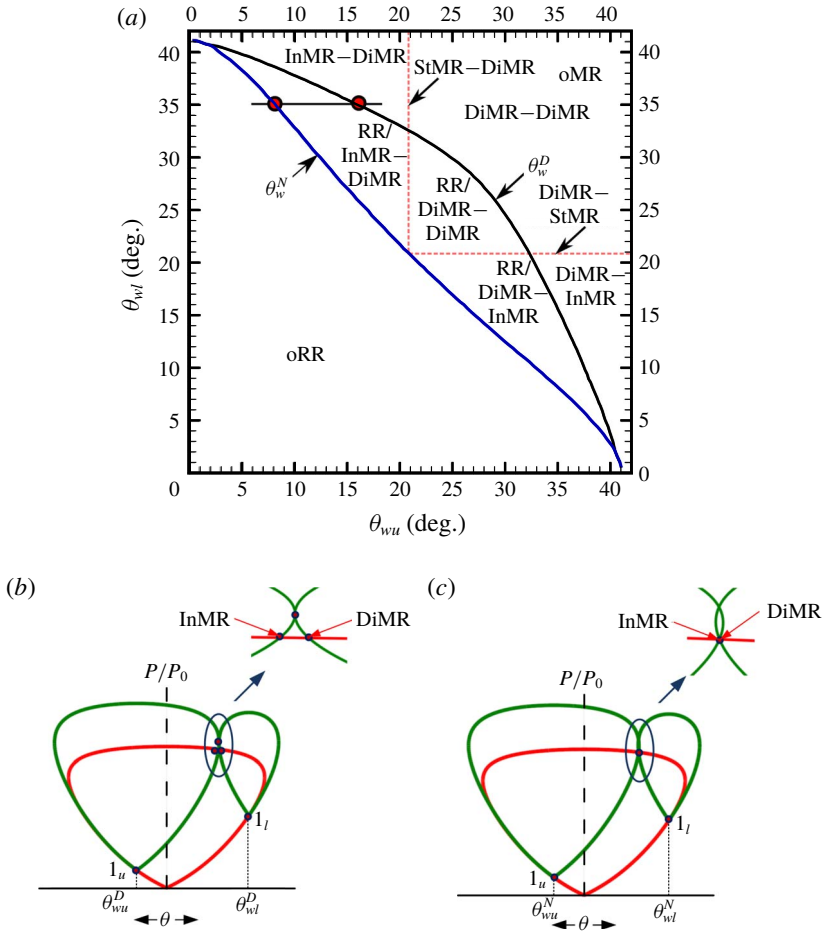

FIGURE 5. (Colour online) (*a*) The dual-solution domain in the $(\theta_{wu}, \theta_{wl})$-plane for $M_0 = 4.96$ (Li *et al.* 1999); (*b*,*c*) shock polars for a set of cases of detachment and von Neumann criteria, respectively.

oMR solutions are possible. Shock polars for arbitrary wedge angles for the two criteria, which are marked in figure 5(*a*), are shown in figure 5(*b*,*c*).

Analytical predictions of InMR configurations have not been addressed by previous work on asymmetric MR by Tao *et al.* (2017), and it is not clear whether their model can correctly predict them. The present work is hence an attempt to develop an analytical model to predict the oMR configurations for all types of steady Mach reflections in asymmetric wedge flows. The present analytical model is based on the Li & Ben-Dor (1997) model for the simple reason that the model takes into consideration most of the physical phenomena in the shock reflection region. For example, in the Li & Ben-Dor (1997) model, the triple point solution, the subsonic region, the reflected shock–expansion-fan interaction and the reflection of the expansion fan from the slip line (although there is no appreciable effect (Henderson 1989)) were considered. Moreover, certain flow features such as the Mach stem, reflected shock configuration and slip-line curvatures were approximated using second-order curves. In the following section, the Li & Ben-Dor (1997) model is discussed, followed

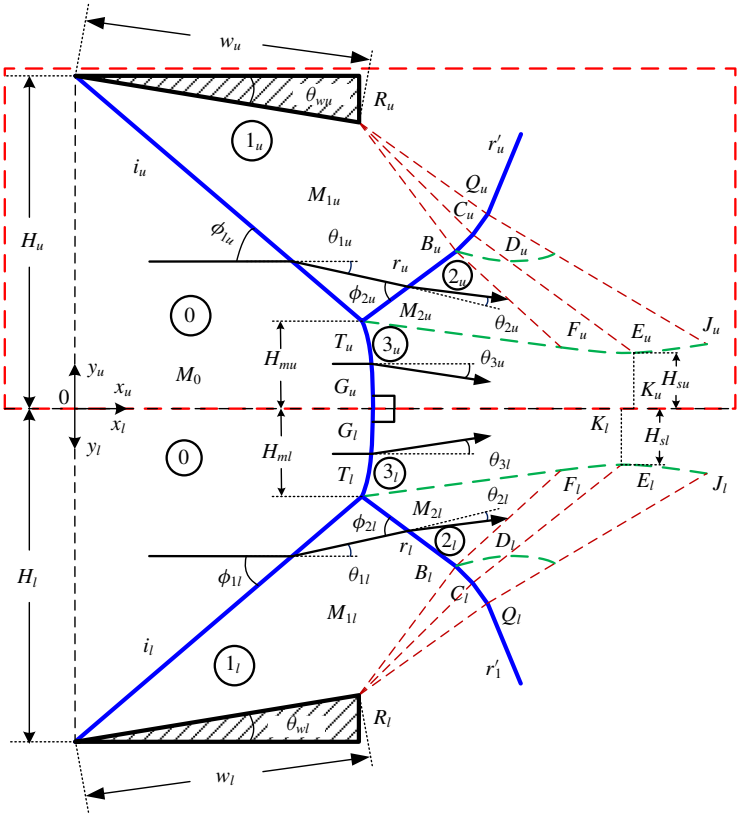

FIGURE 6. (Colour online) Asymmetric MR model (Roy & Rajesh 2017); highlighted symmetric MR model (Li & Ben-Dor 1997).

by some salient features of the Roy & Rajesh (2017) model, which is extended in the present work. Next, the formulation for the present model is given in detail, and finally, the results obtained by this model are presented and analysed. It is expected that the present work will be a useful addition to the more recent interest in asymmetric Mach reflection configurations in steady flows.

2. Base models

The symmetric MR model by Li & Ben-Dor (1997) was an improvement over the ones given by Azevedo (1989) and Azevedo & Liu (1993). The upper part of figure 6 (highlighted in the dashed box) is the schematic of the symmetric MR configuration employed by Li & Ben-Dor (1997). The lower part is added for completeness and the whole schematic represents the model proposed by Roy & Rajesh (2017), and serves as the base model for the present work.

In the Li & Ben-Dor (1997) model, regions of reflection phenomena are systematically solved for unknown parameters. The governing equations for the flow field are combined and rewritten so as to express the flow properties downstream of a shock as functions of upstream flow Mach number M and shock angle ϕ. Flow deflections through expansion waves and the shock–expansion-fan interactions are modelled using the Prandtl–Meyer function. The slip line is taken to be a straight line until

the location where the leading characteristic from the expansion fan interacts with it. The slip line curves downstream of this point to become parallel to the horizontal line of symmetry at a further downstream location. It is at this location that the sonic throat occurs, where the subsonic pocket of the quasi-one-dimensional flow has the minimum area of cross-section. Downstream of the throat, the flow expands further, with the slip lines diverging as well. Thus the expansion fan from the trailing edge of the wedge determines the size and location of the Mach stem by carrying information of the geometrical features through the subsonic pocket to the Mach stem.

A salient feature of the Li & Ben-Dor (1997) model is that the shape of the Mach stem is assumed to be slightly curved, and modelled using a second-order curve as a function of the boundary conditions (coordinates and slope at its ends), under a first-order approximation assuming minimal change in slope. Other similar shapes, such as the curved portion of the slip line and the characteristic lines of the expansion fan in the entropy layer region, are also modelled using this relation. The equation of the curve (Li & Ben-Dor 1997) is as follows:

$$\begin{aligned} J(x, y, x_1, y_1, x_2, y_2, \delta_1, \delta_2) = {} & [(y - y_1)\sin\delta_1 + (x - x_1)\cos\delta_1]^2 \tan(\delta_2 - \delta_1) \\ & + 2[(x_2 - x_1)\cos\delta_1 + (y_2 - y_1)\sin\delta_1][(x - x_1)\sin\delta_1 - (y - y_1)\cos\delta_1] = 0 \end{aligned} \tag{2.1}$$

and the coordinates of the end points $[(x_1, y_1), (x_2, y_2)]$ satisfy the relation:

$$y_2 - y_1 = \tan \Lambda[\delta_1, \delta_2](x_2 - x_1), \tag{2.2}$$

where (δ_1, δ_2) are the slopes (with x-axis) at the ends, and Λ is given by:

$$\Lambda(\delta_1, \delta_2) = \arctan\left[\frac{2\tan\delta_1 + \tan(\delta_2 - \delta_1)}{2 - \tan\delta_1 \tan(\delta_2 - \delta_1)}\right]. \tag{2.3}$$

Roy & Rajesh (2017) proposed the model for asymmetric MR as a combination of upper and lower domains of symmetric MR, as shown in figure 6. Here, the axis of symmetry (for symmetric MR) is taken as the common horizontal x-axis for both the upper and lower domains. By inverting the vertical axis of the coordinate system in the lower domain (y_u to y_l), all the conventions used for the geometrical parameters in the upper domain are retained.

The flow domains around the triple point, and the region of interaction of the expansion fan with the reflected shock, for both the upper and lower domains, were solved independently. The geometrical relations for the upper and lower domains were grouped together to be solved simultaneously, which yielded a set of 23 equations with 24 unknowns. Various possible closing equations were proposed in Roy & Rajesh (2017) and the results for the oMR configurations were compared. Figure 7 gives schematic representations of the closing equations proposed. In figure 7(*a*), the flow in the subsonic pocket is assumed to choke at the same horizontal location, giving a straight vertical line profile to the sonic contour. In figure 7(*b*), the sonic contour is assumed to follow the Mach stem profile by following the exact curvature of the stem. The third approach, which is more fundamental, is shown schematically in figure 7(*c*). Here, it is imposed that the Mach stem has a continuous profile across the upper and lower domains, with the slopes being equal (and perpendicular) at the point of confluence on the axis. This condition for the closing equation was previously concluded to give the best results (Roy & Rajesh 2017), and has been subsequently used in the present study as well.

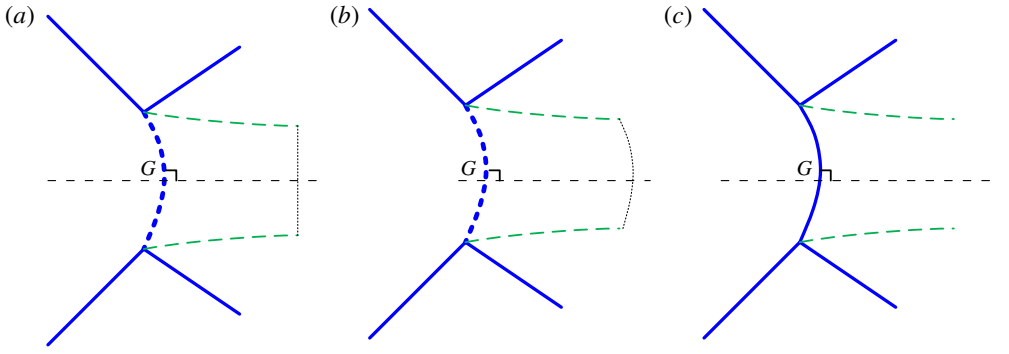

FIGURE 7. (Colour online) Conditions for closing the equations in Roy & Rajesh (2017) model: (*a*) choking at the same abscissa; (*b*) sonic (choking) contour along the Mach stem profile; (*c*) profile continuity of the Mach stem.

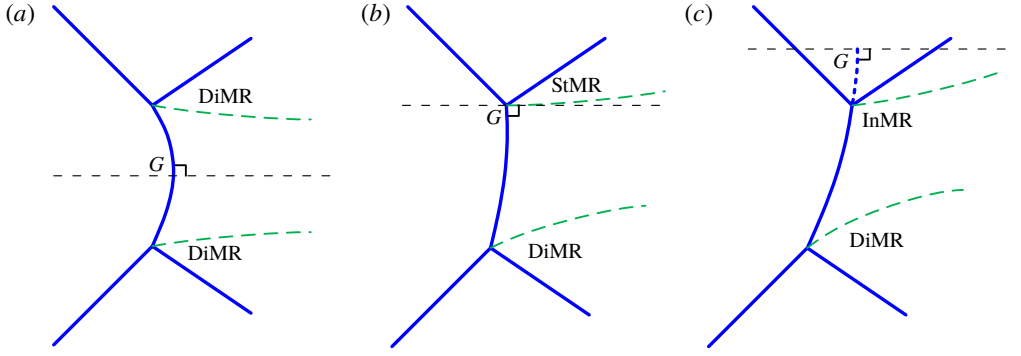

FIGURE 8. (Colour online) Position of common x-axis in Roy & Rajesh (2017) model: (*a*) DiMR–DiMR; (*b*) StMR–DiMR; (*c*) InMR–DiMR (hypothetical).

In the Roy & Rajesh (2017) model, the Mach stem is perpendicular to a common x-axis. It is argued that there is at least one streamline in the uniform flow upstream that passes through the Mach stem without deviation, and this streamline essentially forms the x-axis. The vertical location of the x-axis is variable and depends on the particular case of oMR configuration, as shown in figure 8. In case of DiMR–DiMR, the axis passes through the Mach stem at some intermediate position between the triple points. The axis keeps shifting to any of the triple points for decreasing wedge angle of the corresponding side. The limiting case occurs for StMR–DiMR in which the axis passes through one of the triple points and is also perpendicular to the Mach stem at that point, and the contribution to the Mach stem height is made entirely by the domain on one side of the axis. Although this approach works well for the DiMR–DiMR or DiMR–StMR case, it cannot give the solution for the condition when one of the reflections is an InMR, as shown in figure 8(*c*). Here, the axis becomes perpendicular to the Mach stem at a hypothetically extrapolated location. In this case, the axis cannot be taken as a symmetry plane for any of the symmetric MR halves. This limitation, in particular, has been addressed and resolved in the present work.

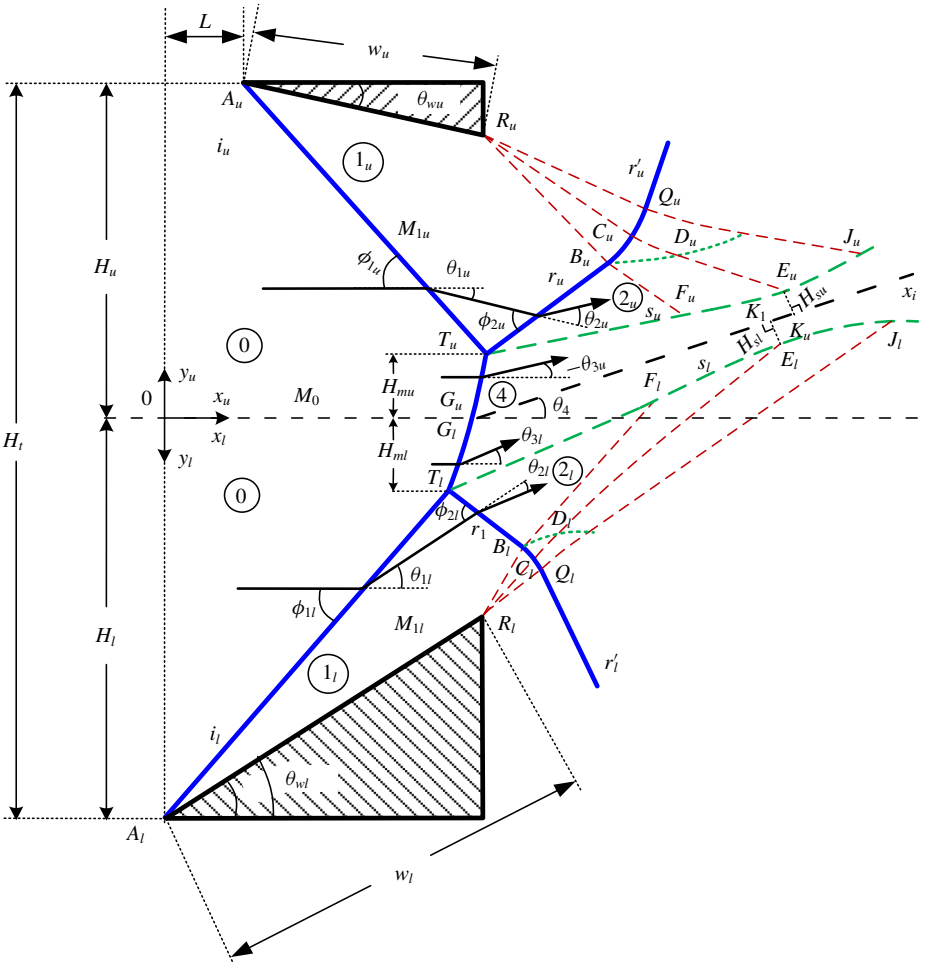

FIGURE 9. (Colour online) Schematic of asymmetric Mach reflection model. H_t is the total height between the wedges. Subscripts u and l depict the upper and lower regions, respectively, with respect to the x axis upstream of the Mach stem and the inclined axis x_i downstream of the Mach stem. H is the height of the leading edge of the wedge, measured from the common horizontal x-axis. The wedge slant length is given as w. H_m is the Mach stem height, i.e. distance of the triple point from the x-axis. H_s is the height of the sonic throat, measured from axis x_i. i is the incident shock, r is the reflected shock, r' is the reflected shock after interaction with the expansion fan, s is the slip line. L is the horizontal gap between the wedges.

3. Formulation of asymmetric MR configuration model

This section contains the detailed formulation for the present asymmetric MR model. The algorithm has been coded in Python, and particularly makes use of the scipy module.

A schematic of the present model is given in figure 9. An inverse MR configuration is given in particular to emphasise the detailed formulation of the present model for InMR cases, while all the other oMR configurations are also analysed. On comparing the present model with the earlier model (Roy & Rajesh 2017) given in figure 6, it is

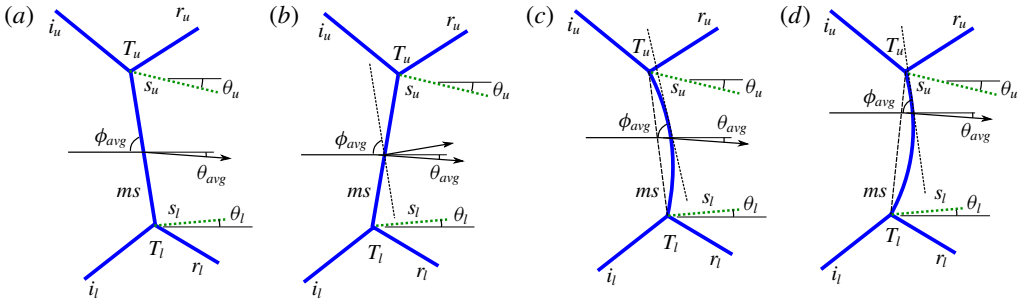

FIGURE 10. (Colour online) Based on theory given by Tao *et al.* (2017), (*a*) $x_{Tu} < x_{Tl}$, (*b*) $x_{Tu} > x_{Tl}$; based on present model, (*c*) $x_{Tu} < x_{Tl}$, (*d*) $x_{Tu} > x_{Tl}$.

to be noted that the subsonic convergent–divergent pocket downstream of the Mach stem, is assumed to be oriented along an inclined axis x_i, rather than parallel to and in continuation with the common horizontal x-axis, where the angle of inclination (θ_4) is the average of the angles at which the streamlines are deflected by the Mach stem at the two triple points. It is argued that at least one streamline from the upstream uniform flow is deflected at this average angle (θ_4) by the Mach stem, at an intermediate location between the two triple points. This incoming streamline before the Mach stem, and its extension beyond the point of deflection, forms the common horizontal x-axis. The direction of the deflected streamline behind the Mach stem is taken to be the inclined axis x_i. Although the subsonic flow behind the Mach stem is known to be non-uniform, the axis x_i indicates the mean orientation of the flow, which is assumed to be quasi-one-dimensional for the present study.

A somewhat seemingly similar approach can be seen in Tao *et al.* (2017). Figure 10 gives a comparison of their approach and that of the present model. Tao *et al.* (2017) employed an average deflection angle θ_{avg}, given by the mean of the slip-line angles with respect to the incoming flow upstream of the Mach stem *ms* near the two triple points T_u and T_l. This is used to calculate the relative locations of the triple points based on the orientation of a straight oblique shock obtained from this average deflection angle. This is shown in figure 10(*a*). It is our understanding that the von Neumann three-shock theory gives only the angles and flow properties near each triple point for given wedge angles, whereas the locations of the triple points are influenced by the geometry and the Mach number of the incoming flow. The geometry comprises of the wedge angles as well as the relative positioning of the wedges. However, in Tao *et al.*'s (2017) model, the θ_{avg} fixes the triple point locations. This is elucidated in figure 10(*b*), where the average flow deflection, which is downward, requires a straight right running oblique shock ($x_{Tu} < x_{Tl}$ as in figure 10*a*) and is shown by the dotted line. However, by virtue of the geometry (location of the wedges), the triple points may be located in such a way that $x_{Tu} > x_{Tl}$, which forms a left running shock. In the present model, this ambiguity is removed by considering the curvature of the Mach stem *ms* which is modelled as a second-order curve using (2.1) to (2.3). Here, the average flow deflection θ_{avg} is used to estimate a location on the curved Mach stem where the inclination would be the same as that of an oblique shock at a shock angle ϕ_{avg}. This accommodates both the cases as shown in figure 10(*c*,*d*). The only difference is that vertical location of x-axis is shifted along the Mach stem.

The governing equations used for this model are based on the assumptions as stated in Li & Ben-Dor (1997). A stable MR configuration exists in the absence of far-field

downstream disturbances. The fluid in consideration is ideal and hence its dynamic viscosity and thermal conductivity are zero. The gas is perfect, with a constant heat capacity ratio γ. The flow in region 2 (see figure 9) is supersonic. The slip lines form a two-dimensional convergent–divergent nozzle, whereby the subsonic flow behind the Mach stem accelerates to become sonic at the throat. Any secondary waves reflected from the slip lines (Gao & Wu 2010; Bai & Wu 2017) have been ignored here, with the understanding that their contribution is not significant in comparison to the primary waves in the overall shock reflection configuration (Ben-Dor 2007, § 2.3.4).

Geometrical inputs required for the model include the total height H_t between the leading edges of the wedges, the slant lengths w_u and w_l of the wedges and the respective deflection angles θ_{wu} and θ_{wl}. The Mach number of the incoming flow is required, along with flow properties such as pressure and temperature from which the thermodynamic state variables are to be calculated.

The region 0 has uniform flow field before the shock structure, and is common to both the upper and lower domains. Region 1 has uniform supersonic flow conditions after being deflected by the incident shock *i*. It extends till the region bound by the leading characteristic of the expansion fan emanating from the trailing edge of the wedge. Region 2 has flow conditions after the flow field passes through the reflected shock *r*. It also extends until and is bound by the leading characteristic of the expansion fan from the trailing edge of the wedge. Region 3 is the area past the Mach stem *ms* and below the slip line *s* and in close vicinity of the triple point *T*. Region 4 lies downstream of the Mach stem, in the vicinity of the *x*-axis, and demarcates the interface of the upper and lower domains at the Mach stem. Subscripts *u* and *l* depict the upper and lower domains, respectively. The equations in the following subsections apply to each of the domains, and have been written without the respective subscripts, unless specifically required.

3.1. *Triple point*

First, we consider the region near the triple points, given in figure 11. The classic von Neumann three-shock theory is applied individually to each triple point, which is the point of confluence of four discontinuities: incident shock *i*, reflected shock *r*, Mach stem *ms* and slip line *s*.

The sign conventions for the angles are as shown in figure 11. Since the vertical axis is inverted for the lower domain, the sign conventions are also reversed. For the general case of DiMR given in figure 11(*c*), the flow deflection angle θ_{3l} is taken to be positive for any deviation of the streamline towards the *x*-axis by a left running shock wave, as in the segment of the Mach stem in this domain. The shock angle ϕ_{3l} is acute. On the other hand, the upper domain given in figure 11(*b*) has an InMR. Following the sign conventions, the flow deflection angle θ_{3u} (depicted as $-\theta_{3u}$ for clarity) is negative. The segment of the Mach stem in this domain is a left running shock wave (instead of a right running wave if it were a DiMR). Hence, in accordance with the mathematics, the shock angle ϕ_{3u} is taken as obtuse. (The angle would be acute for DiMR and 90° for StMR.)

The following equations are used to relate the downstream properties (*j*) to the upstream ones (*i*) across an oblique shock. The details of these relations, which are derived from the conservation equations, can be found in Li & Ben-Dor (1997) and Ben-Dor (2007). Here the flow properties are – Mach number M, shock angle ϕ,

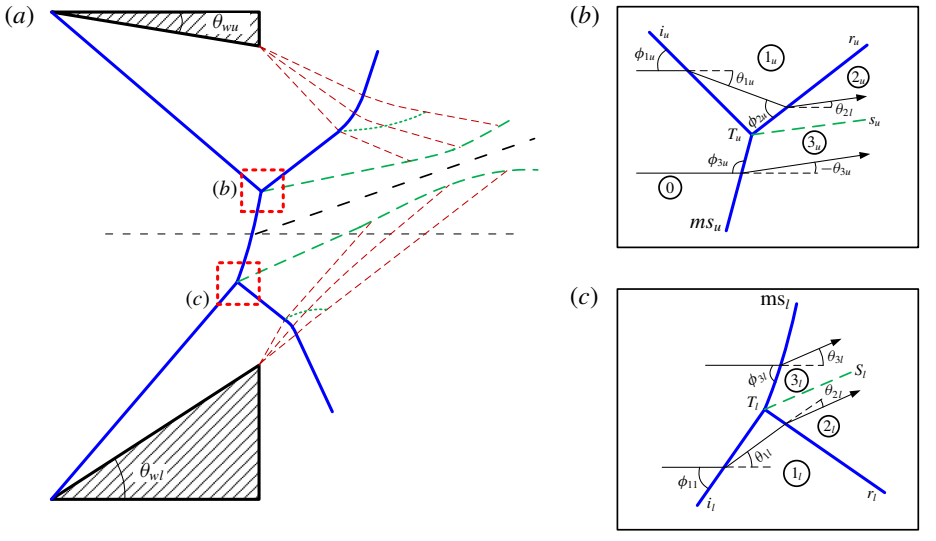

FIGURE 11. (Colour online) (*a*) Schematic of asymmetric MR; insets (*b*) upper triple point region, and (*c*) lower triple point region.

pressure P, flow deflection angle θ, density ρ and local acoustic speed a.

$$\left.\begin{array}{rcl} M_j &=& F(M_i, \phi_j) \\ \theta_j &=& G(M_i, \phi_j) \\ P_j &=& P_i H(M_i, \phi_j) \\ \rho_j &=& \rho_i E(M_i, \phi_j) \\ a_j &=& a_i A(M_i, \phi_j) \end{array}\right\} \sigma_j = \sigma_i \Pi(M_i, \phi_j), \tag{3.1}$$

where, the functions are given as,

$$F(M, \phi) = \left[\frac{1 + (\gamma - 1)M^2 \sin^2\phi + \left[\dfrac{(\gamma+1)^2}{4} - \gamma \sin^2\phi\right] M^4 \sin^2\phi}{\left[\gamma M^2 \sin^2\phi - \dfrac{\gamma - 1}{2}\right]\left[\dfrac{\gamma - 1}{2} M^2 \sin^2\phi + 1\right]}\right]^{1/2} \tag{3.2a}$$

$$G(M, \phi) = \arctan\left[2 \cot\phi \frac{M^2 \sin^2\phi - 1}{M^2(\gamma + \cos 2\phi) + 2}\right] \tag{3.2b}$$

$$H(M, \phi) = \frac{2}{\gamma + 1}\left[\gamma M^2 \sin^2\phi - \frac{\gamma - 1}{2}\right] \tag{3.2c}$$

$$E(M, \phi) = \frac{(\gamma + 1)M^2 \sin^2\phi}{(\gamma - 1)M^2 \sin^2\phi + 2} \tag{3.2d}$$

$$A(M, \phi) = \frac{[(\gamma - 1)M^2 \sin^2\phi + 2]^{1/2}[2\gamma M^2 \sin^2\phi - (\gamma - 1)]^{1/2}}{(\gamma + 1)M \sin\phi}. \tag{3.2e}$$

Across the incident shock i, we have:

$$\sigma_1 = \sigma_0 \Pi(M_0, \phi_1). \tag{3.3}$$

Then, across the reflected shock r, we have:

$$\sigma_2 = \sigma_1 \Pi(M_1, \phi_2). \tag{3.4}$$

And, across the Mach stem ms, we have:

$$\sigma_3 = \sigma_0 \Pi(M_0, \phi_3). \tag{3.5}$$

It is to be noted here that weak shock solutions for (3.3) and (3.4), and strong shock solutions for (3.5), are to be considered.

Finally, we have the following boundary conditions:

$$\theta_1 = \theta_w, \quad P_3 = P_2 \quad \text{and} \quad \theta_3 = \theta_1 - \theta_2. \tag{3.6a–c}$$

The above set of 18 equations are solved for the 18 unknowns: M_1, M_2, M_3, P_1, P_2, P_3, ϕ_1, ϕ_2, ϕ_3, θ_1, θ_2, θ_3, ρ_1, ρ_2, ρ_3, a_1, a_2 and a_3.

For the particular configuration of MR shown in figures 9 and 11, the solution would yield a negative value of θ_{3u} in the upper domain. This negative value is in accordance with the sign convention and is to be retained as such.

While solving the region around the triple points in the upper and lower domains, it is not particularly required to include equations for ρ and a in the set to be solved simultaneously; the set of equations would otherwise contain 12 equations and 12 unknowns, and could be solved nevertheless. However, these quantities are being solved for, as they are required in the upcoming subsection.

As evident from the formulation above, each region around a triple point can be solved for, independent of other geometric and/or physical constraints. Consequently, the angle of deflection of the slip line from the x-axis (and hence the classification among DiMR, StMR or InMR) at either of the triple points is independent of the other.

3.2. *Subsonic pocket downstream of the Mach stem*

3.2.1. *Average deflection at the Mach stem*

As stated earlier, the inclination of the axis x_i is based on an average deflection of the flow by the Mach stem, given as:

$$\theta_4 = \theta_{avg} = \frac{(-\theta_{3u}) + \theta_{3l}}{2}. \tag{3.7}$$

The opposite signs of θ for regions 3_u and 3_l are evoked so as to comply with the flipped y-axes (and sign conventions) of the upper and lower domains. In this subsection, a positive sign is given to angles measured anticlockwise, as for θ_4 and θ_{3l}.

With the Mach stem being modelled as a monotonic second-order curve with continuous slope and no inflection point (using (2.1)–(2.3)), there exists exactly a single location on the Mach stem at which the incoming streamline is deflected by θ_4. This location is named G, as given in figure 9. The x-axis passes through this point on the Mach stem, while its location on the Mach stem itself (given by H_u and H_l) is a variable as of yet.

To keep in line with the sign conventions of each domain, we henceforward redefine θ_4 as:

$$\theta_{4'u} = -\theta_4 \quad \text{and} \quad \theta_{4'l} = \theta_4. \tag{3.8a,b}$$

3.2.2. *Average flow properties behind the Mach stem*

With θ_4 known, the following 5 equation set is solved for the 5 downstream properties, at some intermediate location G on the Mach stem: ϕ_4, M_4, P_4, ρ_4 and a_4. Again, strong shock solution is taken for this case.

$$\sigma_4 = \sigma_0 \Pi(M_0, \phi_4). \tag{3.9}$$

Following Li & Ben-Dor (1997), the average Mach number ($\overline{M}$) behind the Mach stem segments for each domain is defined based on the average velocity ($\overline{u}$) and average acoustic speed ($\overline{a}$), and is given as:

$$\overline{M} = \overline{u}/\overline{a}, \tag{3.10}$$

where a first-order approximation is applied for the following averaging:

$$\overline{u} = \frac{1}{H_m \rho} \int_0^{H_m} \rho u.e_x \, \mathrm{d}y = \frac{1}{2\overline{\rho}} (\rho_3 u_3 \cos\theta_3 + \rho_4 u_4 \cos\theta_4) \tag{3.11}$$

$$\overline{a} = \tfrac{1}{2}(a_3 + a_4) \quad \text{and} \quad \overline{\rho} = \tfrac{1}{2}(\rho_3 + \rho_4). \tag{3.12a,b}$$

Hence, for the subsonic region behind the Mach stem, we have:

$$\overline{M} = \frac{2(\rho_3 u_3 \cos\theta_3 + \rho_4 u_4 \cos\theta_4)}{(\rho_3 + \rho_4)(a_3 + a_4)}, \tag{3.13}$$

where the velocities are given as,

$$u_3 = M_3 a_3 \quad \text{and} \quad u_4 = M_4 a_4. \tag{3.14a,b}$$

The cosine function in the above relations lets us ignore the differing signs (positive or negative) in the two domains for θ_{3u}, θ_{3l} and θ_4.

3.3. *Expansion-fan interaction region*

The regions of interaction of the expansion fans with the reflected shocks, r, are given in figures 12 and 13. The inclination of the subsonic pocket (along axis x_i) by angle θ_4 is included as an angle correction, in the sense that the streamlines are shown to become parallel to x_i rather than x, after interacting with a portion of the expansion fan (Li & Ben-Dor 1997; Ben-Dor 2007). The slip line also follows the curvature of the weak tangential discontinuity (originating from point B) which is one among an infinite number of such entropy layers. The pressure and flow direction remain constant across each layer. Details of the analytical study of expansion-fan interaction with a shock wave can be found in Li & Ben-Dor (1996). Beyond the characteristic line *RCD* of the centred expansion fan, where the flow for the most part assumes a common inclination θ_4, further influence of the expansion fan is ignored as the flow downstream of the throat becomes supersonic and properties there do not influence the upstream flow any further.

Consider the point where the characteristic line *RCD* interacts with the reflected shock r. The point upstream of the shock is labelled as C, and the point downstream as C'. Here, μ is the Mach angle made by the characteristic line at that point. The angle between the flow direction and axis x_i at C, is given as α.

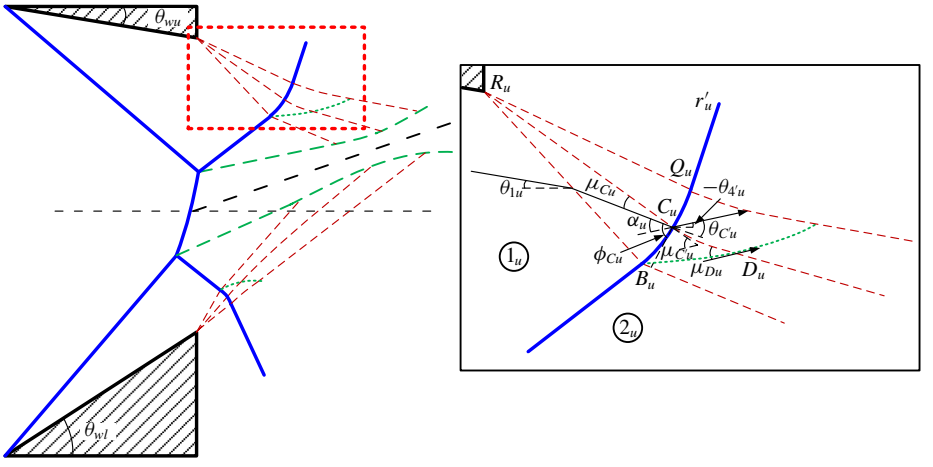

FIGURE 12. (Colour online) Schematic of asymmetric MR: inset; expansion fan interacting with reflected shock wave in upper domain.

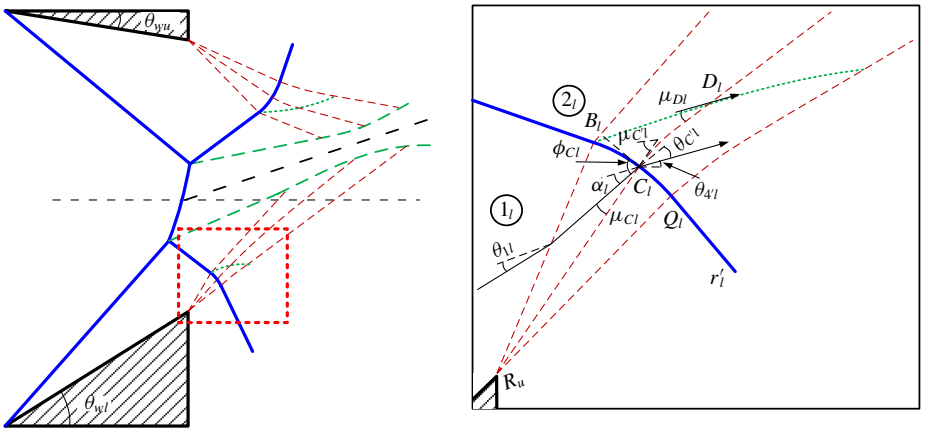

FIGURE 13. (Colour online) Schematic of asymmetric MR: inset; expansion fan interacting with reflected shock wave in lower domain.

Firstly, the Prandtl–Meyer relation is applied between a location in region 2 and point D. The net change in the flow direction here is $\theta_3 - \theta_{4'}$, where $\theta_{4'}$ assumes the value of $\theta_{4'u}$ or $\theta_{4'l}$ as given in (3.8). The pressure remains constant across the parallel entropy layers. Hence, we have the following relations for M_D, P_D and $P_{C'}$.

$$\theta_3 - \theta_{4'} = \nu(M_D) - \nu(M_2), \quad P_D = P_2\chi(M_2, M_D), \quad \text{and} \quad P_{C'} = P_D, \tag{3.15a–c}$$

where ν is the Prandtl–Meyer function and χ is an isentropic function relating the pressures across an expansion fan, given as follows,

$$\nu(M) = \left(\frac{\gamma+1}{\gamma-1}\right)^{1/2} \arctan\left[\frac{(\gamma-1)(M^2-1)}{\gamma+1}\right]^{1/2} - \arctan(M^2-1)^{1/2} \tag{3.16}$$

$$\chi(M_i, M_j) = \left[\frac{2+(\gamma-1)M_i^2}{2+(\gamma-1)M_j^2}\right]^{\gamma/(\gamma-1)}. \tag{3.17}$$

Now, consider a location in region 1, and point C. The Prandtl–Meyer function can be applied again for a change in flow direction by angle $\theta_1 - (\alpha + \theta_{4'})$. Standard relations can be applied across shock r at points C and C'. Hence, the following set of 6 equations are solved for the 6 remaining unknowns: M_C, $M_{C'}$, P_C, ϕ_C, $\theta_{C'}$ and α.

$$\nu(M_C) - \nu(M_1) = \theta_1 - (\alpha + \theta_{4'}), \quad P_C = P_1 \chi(M_1, M_C), \tag{3.18a,b}$$

$$M_{C'} = F(M_C, \phi_C), \quad P_{C'} = P_C H(M_C, \phi_C), \tag{3.19a,b}$$

$$\theta_{C'} = G(M_C, \phi_C), \quad \text{and} \quad \alpha = \theta_{C'}. \tag{3.20a,b}$$

The flow parameters calculated herewith, can now be applied to solve for the geometrical relations.

3.4. *Flow in the subsonic pocket and geometrical relations*

The boundary conditions at the interface apply to both the upper and lower domains, and hence the set of equations in this subsection have to be solved simultaneously.

Consider the subsonic pocket *TFEKG* in figure 9. Here, the cross-sectional area of the pocket at the Mach stem is approximated as the vertical height of the Mach stem H_m. H_s is the perpendicular area of the cross-section at the throat i.e. EK. In order to evaluate H_s, certain geometric manipulations are employed. The details of the geometric relations and the set of equations employed for this subsection are detailed in appendix A.

It is to be noted here that the leading edges of the two wedges have been considered to have a horizontal gap L and the same has been included while calculating the corresponding abscissae. L is to be set to zero where the leading edges are required to be at the same horizontal location.

The quasi-one-dimensional analysis and the geometrical relations along with the closing equations, yield a total of 26 equations with 26 unknowns, including H_{mu} and H_{ml}, from which we get the total height of the Mach stem.

$$H_{mt} = H_{mu} + H_{ml}. \tag{3.21}$$

Finally, the coordinates of the points obtained from the solution are used to reconstruct the entire oMR configuration. Further discussion on this is given in § 4.3.

4. Results and discussion

4.1. *Symmetry case verification*

Due to the nature of the algorithm used herein, the asymmetric MR formulation is expected to predict symmetric MR cases as well. Hence, the data of non-dimensional Mach stem height for symmetric MR are compared with those of the present model in table 1 and figure 14. It follows from symmetry that for equal upper and lower wedge angles, the shock reflection configuration for any mathematical model would be identical in the upper and lower domains. The comparison has hence been made with symmetric half-models by taking half of the height of the Mach stem H_{mt} and that between the wedges H_t.

The data reported in table 1 and figure 14 are taken from Gao & Wu (2010). From table 1, it can be seen for cases 5 and 6 that the present model gives better, if not

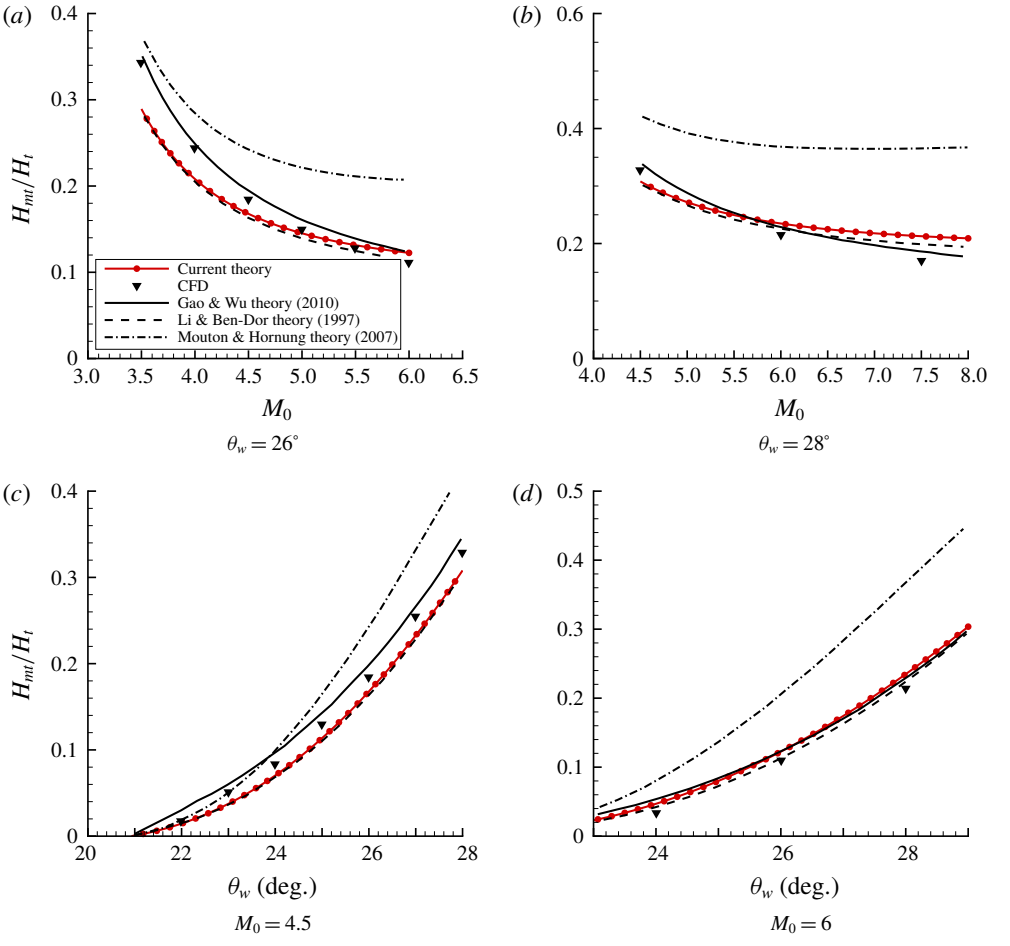

FIGURE 14. (Colour online) Comparisons of non-dimensional Mach stem height, H_{mt}/H_t, from current theory with those of Gao & Wu (2010), Li & Ben-Dor (1997) and Mouton & Hornung (2007), and numerical results from Gao & Wu (2010); $w/H_t = 1.1$.

					H_{mt}/H_t				
Case	M_0	θ_w	ϕ_1	w/H_t	Present	Analytical[a]	Analytical[b]	Analytical[c]	Numerical[c]
1	2.84	20.8	40.1	1.42	0.1175	0.118	0.140	0.202	0.191
2	4.00	23.0	36.0	1.28	0.0767	0.076	0.106	0.110	0.121
3	4.00	25.0	38.5	1.19	0.1704	0.167	0.300	0.213	0.223
4	4.50	23.0	34.5	1.10	0.0376	0.036	0.051	0.058	0.052
5	4.96	28.0	39.7	1.10	0.2742	0.269	0.395	0.292	0.283
6	5.00	26.9	38.2	1.10	0.1974	0.191	0.296	0.213	0.203

TABLE 1. Comparison of the non-dimensional Mach stem height, H_{mt}/H_t, with the values from [a]Li & Ben-Dor (1997), [b]Mouton & Hornung (2008) and [c]Gao & Wu (2010). All angles are in degrees.

the best, agreement with the numerical data. From figure 14, it is evident that the present model (and that of Li & Ben-Dor (1997)) shows excellent agreement with numerical results towards higher Mach numbers ($M_0 > 4.5$). In selected cases, the present theory performs even better than that of Gao & Wu (2010). The Mouton (2007) theory deviates from the numerical data at such high Mach numbers. At lower Mach numbers, there is considerable under-prediction of the Mach stem height by the present model. Since the primary distinction of the Gao & Wu (2010) model is the consideration of secondary waves in the MR configuration, the above analysis suggests that ignoring the secondary waves leads to large errors at low Mach numbers. However, the extent of their contribution at higher Mach numbers needs to be further considered, since we see very good agreement with the numerical data for a certain range, and some over-prediction beyond that (figure 14*a*,*b*).

It can also be noted from table 1 and figure 14 that there exists some discrepancy between the present data and those reported in Li & Ben-Dor (1997). A closer scrutiny revealed a possible error in the algorithm reported in the latter (see Li & Ben-Dor 1997, C9, the appendix). The sign of the angle θ_3 is incorrect, and the same has been corrected in the present theory in (A 12). It has separately been verified that for the symmetric case, the present asymmetric formulation gives exactly the same results as the corrected Li & Ben-Dor (1997) model.

4.2. *Variation of Mach stem height*

Using the present algorithm, the wedge-angle-variation-induced changes in the Mach stem height have been estimated for a series of cases. Also, the wedge angles at which the Mach stem height becomes zero is in direct conformation to the von Neumann criterion. It is to be noted however that each value calculated using the present theory is a steady-state result. There is no dynamic effect (Naidoo & Skews 2014) associated with changing wedge angles in this analytical model.

For all calculations in this subsection, the Mach number M_0 has been taken to be 4.96. The geometric parameters have been taken following Li *et al.* (1999). The vertical height between the wedges is 71 mm and the wedges are of equal slant height at 40 mm each. The total pressure is taken to be 8.5 bar and the total temperature is 473 K. (These parameters are required as input to the algorithm. However, except the Mach number and geometrical parameters, other flow properties are dealt with as ratios across the discontinuities, and can be arbitrarily assumed within the perfect and ideal gas assumptions.) The above parameters ensure that oMR is possible for a range of angles in such a flow field, as determined from experimental results. The horizontal gap L between the wedges is zero.

In figure 15, the transitions from oMR $\rightarrow$ oRR have been shown for various types of initial oMR configurations. The cases taken here are symmetric DiMR–DiMR with equal wedge angles changing along the path (*c*), asymmetric DiMR–DiMR with unequal wedge angles varying along a straight line path (*d*), StMR–DiMR with constant upper wedge angle (symmetric θ_w^N) and varying lower wedge angle along the path (*e*) and, lastly, InMR–DiMR with unequal wedge angles varying along the straight line path (*f*). Figures 15(*c*) through 15(*f*) represent shock polars for the paths as indicated in figure 15(*a*), and the normalised Mach stem heights versus the lower wedge angles for these cases are given in figure 15(*b*). Solution points have been marked in colour in all the corresponding plots for each of the cases – only oMR, dual-solution (ds) domain and von Neumann (vN) criterion. A global sign convention for wedge angles is adopted for the shock polars here, whereby

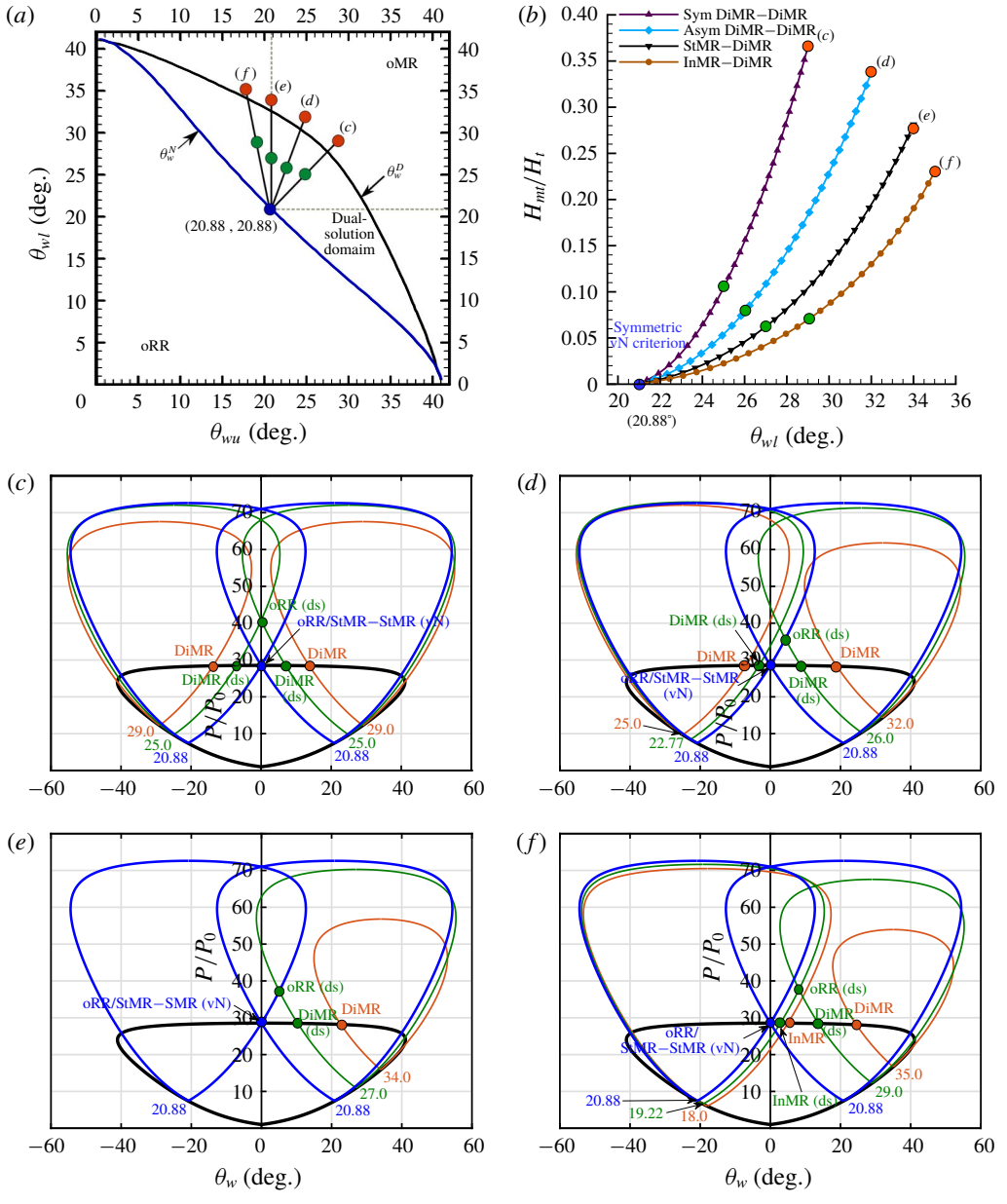

FIGURE 15. (Colour online) Symmetric von Neumann criterion for $M_0 = 4.96$. (*a*) The dual-solution domain in the (θ_{wu}, θ_{wl})-plane (Li *et al.* 1999); (*b*) plots of normalised Mach stem height versus lower wedge angle; (*c*) shock polars for symmetric DiMR–DiMR case; (*d*) shock polars for asymmetric DiMR-DiMR case; (*e*) shock polars for asymmetric StMR-DiMR; (*f*) shock polars for asymmetric InMR-DiMR case.

anticlockwise rotation as for the lower wedge is taken to be positive, and clockwise rotation as for the upper wedge is taken to be negative.

All the plots in figure 15 converge at the symmetric von Neumann point, which for M_0 of 4.96 occurs at 20.88°. There is excellent agreement of the analytically predicted

					Asymmetric	Symmetric			
Case	θ_{wu}	θ_{wl}	ϕ_{1u}	ϕ_{1l}	H_{mt}/H_t	θ_w	ϕ_1 (equiv.)	H_{mt}/H_t	Difference (%)
DiMR	22.4	25.0	32.69	35.85	0.053936	23.7	34.267	0.054305	0.684
StMR	20.9	25.0	30.88	35.86	0.032166	23.0	33.371	0.033056	2.767
InMR	20.0	25.0	29.92	35.87	0.022526	22.6	32.890	0.023743	5.402

TABLE 2. Comparison of the non-dimensional Mach stem height, H_{mt}/H_t, from the present theory for various asymmetric cases with corresponding symmetric case, based on the equivalence shock angle concept (Mouton 2007). All angles are in degrees.

value as confirmed from theory from the (θ_{wu}, θ_{wl})-plane and the shock polars. It is interesting to note that both the wedge angles would be equal at the symmetric von Neumann point, and this point hence, is a theoretical StMR–StMR configuration. However, the Mach stem height is zero at this point, and this denotes a transition to oRR.

It is interesting to note from figure 15(*b*) that the highest Mach stem heights are obtained for the symmetric case, and the Mach stem heights for corresponding lower wedge angles become smaller as one moves away from symmetry. It is easy to extrapolate from symmetry that plots on the other side of symmetry line (*c*) in the (θ_{wu}, θ_{wl})-plane would bear the same pattern.

It is also plausible to comment from this analysis that any approximation of an asymmetric MR to a symmetric MR (concept of equivalence shock angle, (Mouton 2007, chap. 5, 9)) would result in estimation of Mach stem height higher than the actual value. To elucidate this, table 2 lists the Mach stem heights for the various types of oMRs on paths *d*, *e* and *f*, and those for the corresponding equivalence shock angle on path *c*, in figure 15(*b*). It is seen that the difference increases with asymmetry, with the highest for InMR. For near-symmetric wedge angles as in the DiMR case, however, the difference is quite small, corroborating that proposed in Mouton (2007).

The salient feature of this work is the prediction of the InMR configurations. To see how accurate the present model predicts these configurations, cases of InMR–DiMR have been considered here in figure 16, whereby the upper wedge angle is retained at 18° and the lower wedge angle is reduced until the von Neumann condition at 23.84°. The path is shown on the (θ_{wu}, θ_{wl})-plane in figure 16(*a*), the Mach stem height in figure 16(*b*), and the corresponding shock polars in figure 16(*c*). It can be seen that the von Neumann condition is accurately predicted at θ_{wl} of 23.84°, as obtained from the shock polar theory.

4.3. *Asymmetric MR configurations*

The coordinates of various points obtained as solutions from the algorithm are used to render the oMR configuration. Here, (2.1) is used to interpolate points for the curved entities – Mach stem, and portions of the slip lines, expansion-fan characteristic lines and reflected shocks.

The configuration obtained from the present model has been validated with numerical and experimental results in this section. As mentioned earlier, cases of highly asymmetric configurations such as those of InMR, are especially considered.

In figure 17, the plots corresponding to an inverse Mach reflection, in particular oMR(DiMR+InMR), for an upper wedge angle θ_{wu} of 28° and lower wedge angle θ_{wl} of 18°, are shown. The wedge angles chosen correspond to an InMR–DiMR in

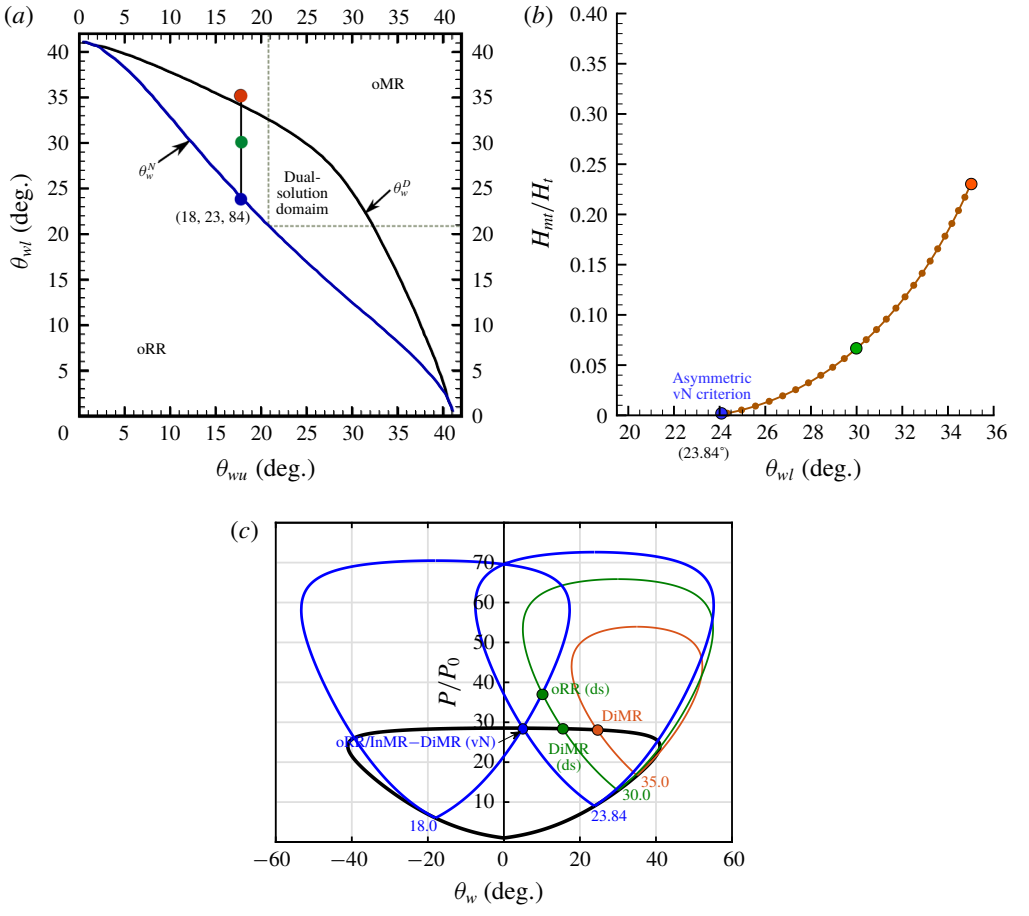

FIGURE 16. (Colour online) Asymmetric von Neumann criterion for $M_0 = 4.96$. (*a*) The dual-solution domain in the $(\theta_{wu}, \theta_{wl})$-plane (Li *et al.* 1999); (*b*) plot of normalised Mach stem height versus lower wedge angle for InMR-DiMR; (*c*) shock polars for asymmetric InMR-DiMR case.

the dual-solution domain on the $(\theta_{wu}, \theta_{wl})$-plane, as can be seen from figure 16(*a*). In figure 17(*a*), the predicted configuration has been overlapped upon a colour schlieren photograph of an oMR for the same wedge angles, given in Li *et al.* (1999). It can be seen that the predicted oMR configuration matches very well with the experimental oMR configuration. The rather small size of the Mach stem makes it difficult to visualise the area close to the stem. A zoomed-in view is therefore presented in figure 17(*b*). The line plots for various features such as shocks, characteristic lines of the expansion fan, slip line and streamline, are differentiated with colour. (The coordinate system shown in figure 17(*b*) corresponds to the approach primarily adopted in the present algorithm. For the latter plots, the axes have been shifted vertically down by H_l.)

It may be noted that the streamline direction downstream of the Mach stem is fictitious, as the flow is no longer uniform. The streamline represents the general flow direction and inclination of the subsonic pocket, or more correctly, axis x_i of the present model. The slip lines become parallel to x_i at their respective choking sections

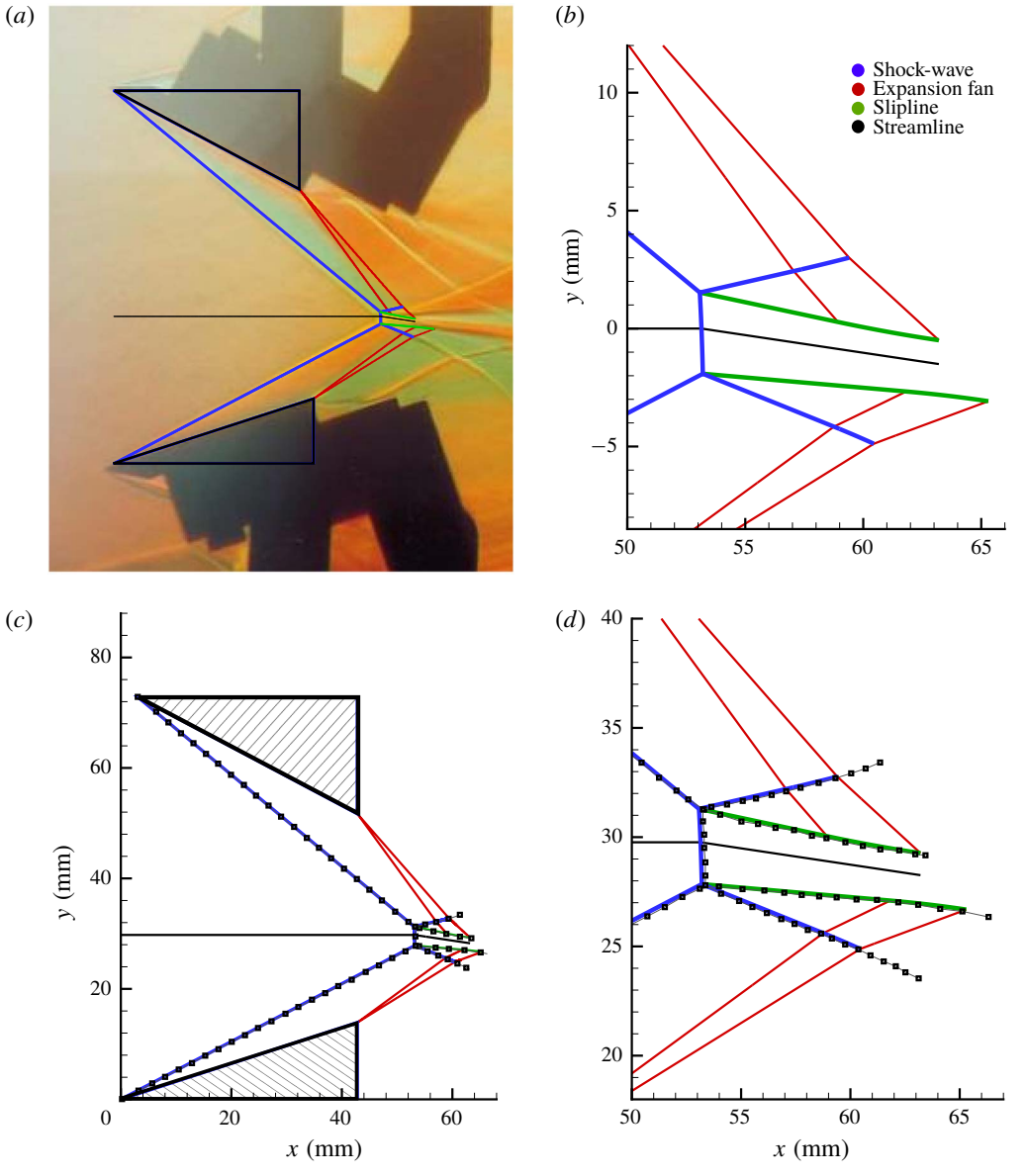

FIGURE 17. (Colour online) Comparison of inverse Mach reflection (DiMR–InMR) configuration at $M_0 = 4.96$ for $(\theta_{wu}, \theta_{wl}) = (28°, 18°)$ with present model (line plot). (*a*) Comparison with colour schlieren (Li *et al.* 1999); (*b*) zoomed-in view of the Mach stem region; (*c*) comparison with data from numerical results, marked with □ (Ivanov *et al.* 2002); (*d*) zoomed-in view of the Mach stem region in plot c.

(part of the boundary conditions in the model) which is reasonable in the context of the experimental observations of such flow fields.

In figure 17(*c*,*d*), the predicted results have been compared with numerical data presented in Ivanov *et al.* (2002). Here, the trailing edges of the two wedges are at the same horizontal location, unlike the leading edges as in the case of Li *et al.* (1999).

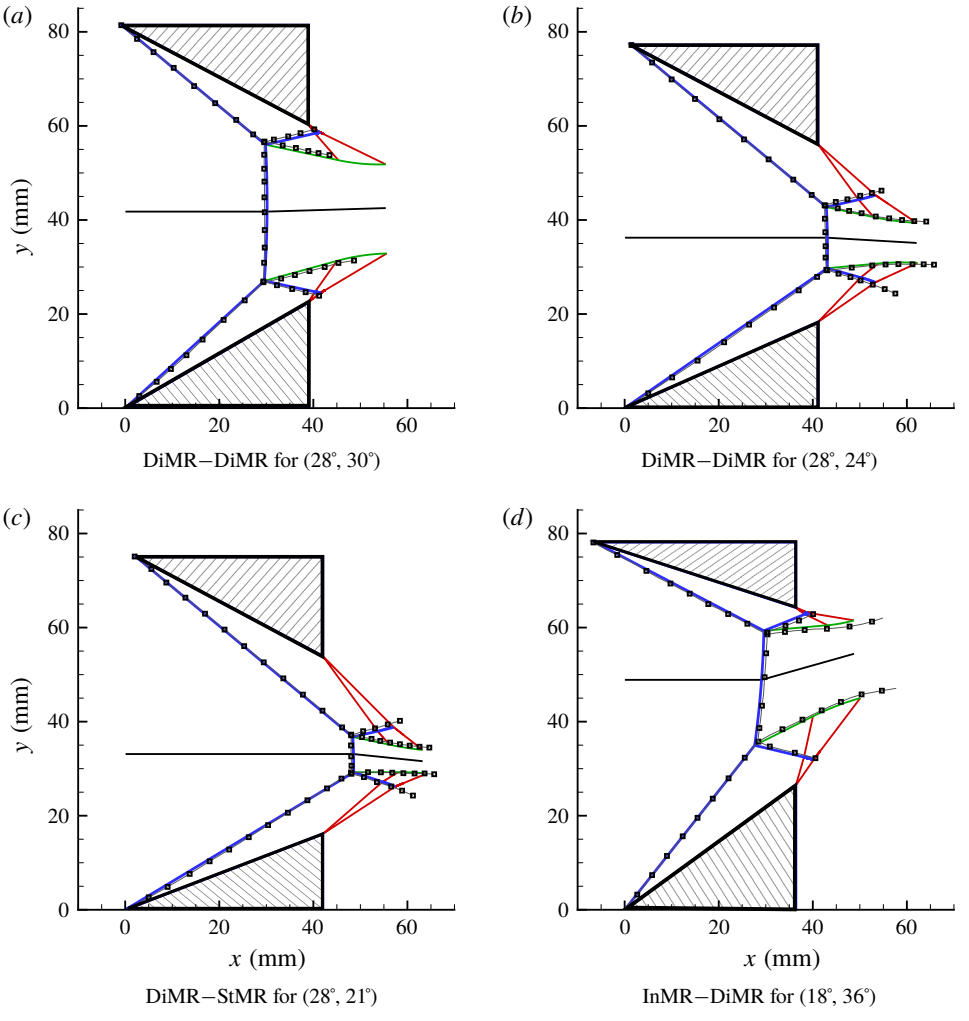

FIGURE 18. (Colour online) Comparison of oMR configurations with present model (line plot) with data from numerical results for $M_0 = 4.96$, marked with □ (Ivanov *et al.* 2002).

The two data sets have been scaled and mapped by matching the leading and trailing edges of the wedges. The agreement is seen to be quite good, with a clearer picture being provided by the magnified view.

The present model is known to predict a discontinuity between the upper and lower sections at the choking location. This is likely to become predominant at large asymmetric wedge angles owing the deviation from the quasi one-dimensional assumption used in the present formulation. However, it can be seen from the plots that the agreement between the computational and analytical data is quite good despite the fact that the asymmetry in wedge angles is large, indicating the reliability of the present model even for highly distorted oMR configurations.

Further cases of asymmetric MR have been given in figure 18, to compare the profiles of the present configurations with numerical results of Ivanov *et al.* (2002). Figure 18(*a*) shows a direct MR (DiMR–DiMR) case with (θ_{wu}, θ_{wl}) as (28°, 30°).

The oMR configuration is more asymmetric in figure 18(*b*), but the configuration is still a direct MR. Figure 18(*c*) shows a case of stationary MR (DiMR–StMR), whereby the slip line for the lower domain emerges parallel to the incoming flow direction at the triple point. Lastly, figure 18(*d*) shows an inverse MR (InMR–DiMR) with a substantial height of the Mach stem. This configuration clearly reveals the profile of the Mach stem. The agreement with the numerical data is excellent for the above cases, though close inspection reveals that the present model under-predicts the Mach stem height by a small margin for cases (*a*), (*b*) and (*c*), while slightly over-predicting for case (*d*). The Mach stem profile is accurately captured, as seen in cases (*a*) and (*d*).

5. Conclusion

The analytical formulation presented in this paper predicts the overall configuration of an asymmetric Mach reflection for all the possible oMR configurations. The model successfully predicts the profile of the waves and wave interactions in the oMR configurations. The present model takes into account most of the flow phenomena, such as the curved Mach stem, subsonic pocket and the interaction of the reflected shocks with the expansion fans, that occur in the shock reflections in the asymmetric wedge flows. The Mach stem heights predicted by the model have been validated with several numerical and analytical data available for symmetric cases. The agreement is quite good at high Mach numbers. However, the effects of ignoring secondary waves in the present model at very high Mach numbers need to be further investigated.

The asymmetric Mach stem heights have been computed for various types of oMR configurations. The pattern of variation of Mach stem height with wedge angles, for a Mach number of 4.96, is explored. The von Neumann criterion is found to be satisfied exactly by the present model for both symmetric and asymmetric cases. The highest Mach stem height is obtained when approached on the symmetric path. This suggests that equivalence angles, as employed in some of the previous works to approximate the asymmetric case to symmetric case, will result in over-prediction of the Mach stem height, although the difference is minimal for small asymmetries.

The profile of the overall asymmetric MR configuration is predicted and validated for a Mach number of 4.96 with experimental and numerical data. It is seen that the present model is able to predict the MR configuration with appreciable accuracy. The Mach stem profile is well captured in all cases, including inverse MR.

Appendix A

A.1. *Flow in the subsonic pocket and geometrical relations*

A schematic of the upper domain with the necessary nomenclature is given in figure 19. The lower domain follows a similar description. From figure 19, the following relations are evident based on the geometry. The abscissa of the leading edge of the lower wedge is the same as the origin on the x axis. The upper wedge is at a horizontal gap L, as shown.

$$\left.\begin{array}{c} X_{Au} = L, \quad X_{Al} = 0.0, \quad X_{Ru} = L + w_u \cos\theta_{1u}, \quad X_{Rl} = w_l \cos\theta_{1l}, \\ X_{Tu} = L + (H_u - H_{mu}) \cot\phi_{1u}, \quad X_{Tl} = (H_l - H_{ml}) \cot\phi_{1l}, \\ Y_R = H - w \sin\theta_1, \quad \text{and} \quad Y_T = H_m. \end{array}\right\} \tag{A 1}$$

Consider the subsonic pocket *TFEKG*. The angle β is given by the inverse of the tangent of the ratio of *EN* and *GN*. By adding $\theta_{4'}$ to β (in case of the upper domain,

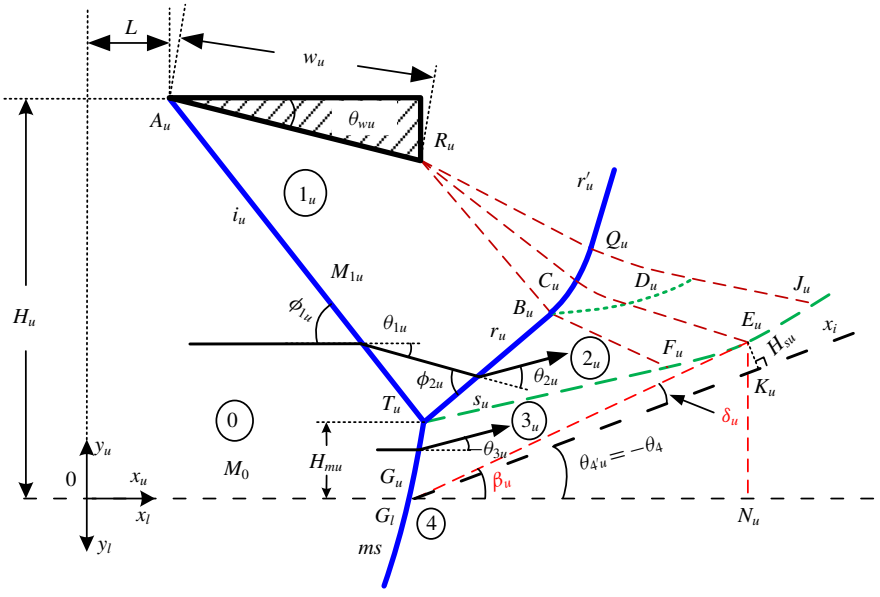

FIGURE 19. (Colour online) Schematic of upper domain of asymmetric MR configuration.

adding $\theta_{4'u} = -\theta_4$ to β_u), we get the angle δ, from which H_s can be obtained using a sin function along with the length EG. The relations are given below.

$$\left.\begin{aligned} \beta = \text{atan}\left[\frac{Y_E}{X_E - X_G}\right], \quad \delta = \beta + \theta_{4'}, \\ \text{and} \quad H_s = \sqrt{(Y_E)^2 + (X_E - X_G)^2}\,\sin\delta. \end{aligned}\right\} \tag{A 2}$$

As mentioned at the beginning of § 3, the sonic contour is not taken to be continuous from E_u to E_l. Rather, the choking throats are approximated as straight cross-sectional areas, perpendicular to the axis x_i, to be better suited to the quasi-one-dimensional assumption here. Results obtained by Roy & Rajesh (2017) show that the MR profile around the Mach stem is disoriented when the sonic contour is imposed to be a continuous straight or slightly curved line. Furthermore, adding boundary conditions of continuity for both the Mach stem and sonic contour over-constrains the set of equations in this subsection.

The average Mach number downstream of the Mach stem *ms* has been calculated in § 3.2.2. Using $\overline{M}$, we apply the quasi-one-dimensional-area–Mach-number relation between H_m and H_s, as follows.

$$\frac{H_m}{H_s} = \frac{1}{\overline{M}}\left[\frac{2}{\gamma+1}\left(1 + \frac{\gamma-1}{2}\overline{M}^2\right)\right]^{(\gamma+1)/2(\gamma-1)}. \tag{A 3}$$

We now advance with a more rigorous consideration of the geometric relations. Refer to figure 19 for the following.

Consider the straight line RB,

$$Y_B - Y_R = -\tan(\mu_B + \theta_1)(X_B - X_R), \quad \text{where } \mu_B = \arcsin(1/M_1) \tag{A 4}$$

consider the straight line RC,

$$Y_C - Y_R = -\tan(\mu_C + \alpha + \theta_{4'})(X_C - X_R), \quad \text{where } \mu_C = \arcsin(1/M_C) \tag{A 5}$$

consider the straight line BF,

$$Y_F - Y_B = -\tan(\mu_F + \theta_3)(X_F - X_B), \quad \text{where } \mu_F = \arcsin(1/M_2) \tag{A 6}$$

consider the straight line DE,

$$Y_E - Y_D = -\tan(\mu_D + \theta_{4'})(X_E - X_D), \quad \text{where } \mu_D = \arcsin(1/M_D) \tag{A 7}$$

consider the straight line TB,

$$Y_B - Y_T = \tan(\phi_2 - \theta_1)(X_B - X_T) \tag{A 8}$$

consider the straight line TF,

$$Y_F - Y_T = -\tan\theta_3(X_F - X_T). \tag{A 9}$$

For curved line segments, we take equations of the form given in (2.2), and use the function in (2.3). It is assumed here that these curvatures are very small. The profile of the curve is a function of the coordinates of its end points and the inclinations (slope with the x-axis) of the curve at the end points.

Consider the curve BC,

$$Y_B - Y_C = \tan\Lambda[(\phi_2 - \theta_1), (\phi_C - \alpha - \theta_{4'})](X_B - X_C) \tag{A 10}$$

consider the curve CD,

$$Y_C - Y_D = \tan\Lambda[(-\arcsin(1/M_{C'}) - \theta_{4'}), (-\arcsin(1/M_D) - \theta_{4'})](X_C - X_D) \tag{A 11}$$

consider the curve BD,

$$Y_B - Y_D = \tan\Lambda[(-\theta_3), (-\theta_{4'})](X_B - X_D) \tag{A 12}$$

consider the curve FE,

$$Y_F - Y_E = \tan\Lambda[(-\theta_3), (-\theta_{4'})](X_F - X_E). \tag{A 13}$$

The set of equations (A 3) to (A 13), considering both the domains, constitute a total of 22 equations and 26 unknowns. Additional equations for boundary conditions have to be added, to close the set of equations. Firstly, we know the relation for the total height between the wedges.

$$H_t = H_u + H_l. \tag{A 14}$$

As discussed earlier in § 2, following Roy & Rajesh (2017) we employ the condition that the Mach stem is required to have a continuous profile between the triple points in the upper and lower domains. Value of ϕ_4 has already been obtained in § 3.2.1.

$$Y_T = \tan\Lambda[(\pi - \phi_3), (\phi_{4'})](X_T - X_G), \quad \text{where } \phi_{4'u} = \phi_4, \phi_{4'l} = \pi - \phi_4. \tag{A 15}$$

And,

$$X_{Gu} = X_{Gl}. \tag{A 16}$$

We now have a total of 26 equations (A 3) to (A 16) for the 26 unknowns (read for both upper u and lower l domains): X_G, Y_T, X_B, Y_B, X_C, Y_C, X_D, Y_D, X_F, Y_F, X_E, Y_E and H. Here, $H_m = Y_T$, from which we get the total height of the Mach stem, and from H we get the location of the x/x_i axes.

REFERENCES

AZEVEDO, D. J. 1989 Analytic prediction of shock patterns in a high-speed, wedge-bounded duct. PhD thesis, State University of New York, New York, NY.

AZEVEDO, D. J. & LIU, C. S. 1993 Engineering approach to the prediction of shock patterns in bounded high-speed flows. *AIAA J.* **31** (1), 83–90.

BAI, C. Y. & WU, Z. N. 2017 Size and shape of shock waves and slipline for Mach reflection in steady flow. *J. Fluid Mech.* **818**, 116–140.

BEN-DOR, G. 2007 *Shock Wave Reflection Phenomena*. Springer.

GAO, B. & WU, Z. N. 2010 A study of the flow structure for Mach reflection in steady supersonic flow. *J. Fluid Mech.* **656**, 29–50.

HENDERSON, L. F. 1989 On the refraction of shock waves. *J. Fluid Mech.* **198**, 365–386.

HENDERSON, L. F. & LOZZI, A. 1975 Experiments on transition of Mach reflexion. *J. Fluid Mech.* **68** (1), 139–155.

HORNUNG, H. G. & MOUTON, C. A. 2008 Some more on transition between regular and Mach reflection of shock waves in steady flow. In *38th Fluid Dyn. Conf. Exhib.*, American Institute of Aeronautics and Astronautics.

HORNUNG, H. G., OERTEL, H. & SANDEMAN, R. J. 1979 Transition to Mach reflexion of shock waves in steady and pseudosteady flow with and without relaxation. *J. Fluid Mech.* **90** (3), 541–560.

IVANOV, M. S., BEN-DOR, G., ELPERIN, T., KUDRYAVTSEV, A. N. & KHOTYANOVSKY, D. V. 2002 The reflection of asymmetric shock waves in steady flows: a numerical investigation. *J. Fluid Mech.* **469**, 71–87.

LI, H. & BEN-DOR, G. 1996 Oblique-shock/expansion-fan interaction – analytical solution. *AIAA J.* **34** (2), 418–421.

LI, H. & BEN-DOR, G. 1997 A parametric study of Mach reflection in steady flows. *J. Fluid Mech.* **341**, 101–125.

LI, H., CHPOUN, A. & BEN-DOR, G. 1999 Analytical and experimental investigations of the reflection of asymmetric shock waves in steady flows. *J. Fluid Mech.* **390**, 25–43.

MOUTON, C. A. 2007 Transition between regular reflection and mach reflection in the dual-solution domain. PhD thesis, California Institute of Technology, Pasadena, CA.

MOUTON, C. A. & HORNUNG, H. G. 2007 Mach stem height and growth rate predictions. *AIAA J.* **45** (8), 1977–1987.

MOUTON, C. A. & HORNUNG, H. G. 2008 Experiments on the mechanism of inducing transition between regular and Mach reflection. *Phys. Fluids* **20** (126103), 1–11.

NAIDOO, K. & SKEWS, B. W. 2014 Dynamic transition from Mach to regular reflection of shock waves in a steady flow. *J. Fluid Mech.* **750**, 385–400.

ROY, S. & RAJESH, G. 2017 Analytical prediction of Mach stem height for asymmetric wedge reflection in 2-D steady flows. In *31st Int. Symp. Shock Waves. Nagoya, Japan*.

TAO, Y., FAN, X. & ZHAO, Y. 2015 Flow visualization for the evolution of the slipstream in steady shock reflection. *J. Vis.* **18**, 21–24.

TAO, Y., LIU, W., FAN, X., XIONG, B., YU, J. & SUN, M. 2017 A study of the asymmetric shock reflection configurations in steady flows. *J. Fluid Mech.* **825**, 1–15.

VON-NEUMANN, J. 1943 Oblique reflection of shocks. In *Explos. Res. Rep. 12*, Navy Department, Bureau of Ordinance.

VON-NEUMANN, J. 1945 Refraction, intersection and reflection of shock waves. In *NAVORD Re 203-45*, Navy Department, Bureau of Ordinance.